Control of Electromechanical Actuators: Valves Tapping in Rhythm

Katherine Peterson[1], Anna Stefanopoulou[1], and Yan Wang[1]

University of Michigan, Ann Arbor MI

Abstract. Electromechanical valve (EMV) actuators can replace the camshaft allowing for electronically controlled variable valve timing (VVT) on a new generation of engines. Through the use of VVT, engine operation can be optimized to allow for improvements in fuel economy, performance, and emissions. Before EMV actuators can be used in production vehicles two critical problems need to be resolved. First, impact velocities between the valve, valve seat, and the actuator itself need to be small to avoid excessive wear on the system and ensure acceptable levels of noise. Second, the opening and closing of the valve needs to be both fast and consistent to avoid collision with the piston and to reduce variability in trapped mass. An extensive control analysis of the EMV actuator and the control difficulties are presented. Finally, a linear, a nonlinear, and a cycle-to-cycle self-tuning controllers are designed and demonstrated on a benchtop experiment.

1 Introduction

The automobiles of the 90's are 10 times cleaner and twice as efficient as the vehicles of 1970's. Despite these improvements the transportation sector is still responsible for a large percentage of the CO_2 and other harmful emission (HC, NO_x, smoke, etc) generated throughout the world. Indeed, the increasing population combined with the strong desire for personal mobility will result in 800 millions registered vehicles worldwide by the year 2020 [4]. More than 18% of these cars will be concentrated in less than 30 cities (megacities) around the world deteriorating urban air quality. The vast majority of these cars will be using Internal Combustion (IC) engines. While potential replacements for the IC engine exist such as electro-chemical propulsion based on fuel cells or batteries, the infrastructure requirements are difficult to achieve.

With these projections in mind one soon realizes the pressing need for clean and efficient internal combustion engines. Indeed, engineers throughout the world are racing ahead in their efforts to improve the internal combustion engine. In this race the well-tuned mechanically connected parts in the IC engine of the past are transformed to electronically controlled mechanisms that provide many degrees of freedom for performance optimization.

Electronically controlled variable valve timing (VVT) is the last frontier in IC engine automation. It allows control of the valve motion independently of the piston motion and thus together with electronic spark timing and injection can optimize the three fundamental combustion variables, namely, ignition timing, fuel and air.

2 Variable Valve Timing Technology

Extensive effort has been and is being made in the design of variable valve control mechanisms at research and development laboratories throughout the world. Several VVT mechanisms are introduced in this section. For an overview of more systems the reader is referred to [1].

In Cam Phasing [9] a mechanism is used to adjust the phase of the camshaft to the crankshaft rotation, and thus, can shift the phase of the valve timing. In Cam Profile Switching [3] and Multi-dimensional Cams [14] two or more camshafts are used to optimize the engine performance. Depending on operating conditions a mechanism switches to the desired cam profile to achieve the best performance.

While such VVT schemes can be found in the market today, the VVT variability that they achieve is small because the mechanisms they employ are extensions of the conventional cam-crank shaft designs. Alternatively electromechanical and electrohydraulic valve actuators can completely eliminate the cam-crank shaft mechanical linkage and allow a wide continuously variable valve timing.

The basic working premise of the electrohydraulic valve actuator is the use of compressed or high pressure fluids to control the valve motion. By governing the fluid flow throughout the actuator, the valve timing and lift can be varied with a high degree of flexibility. In [12] an electrohydraulic actuator is presented that exploits the elastic properties of the compressed hydraulic fluid to provide continuously variable control of engine valve timing, lift, and velocity.

Electromechanical valve actuators, which are the focus of this paper, use magnets as a means to govern the valve motion. The electromechanical valve (EMV) actuator studied in this paper is shown in Fig. 1 and its functionalities are discussed in [6]. The actuator governs the opening/closing of the valve through the forcing of a set of springs and electromagnets. A typical opening/closing cycle is shown in Fig. 1. Initially the armature is held in the closed position by the upper magnetic coil, causing the spring on that side to be more compressed than the opposing spring. At time t_{rc} the release command is given and the voltage across the upper magnetic coil is reduced to zero. The difference in the spring force drives the armature across the 8 mm gap, thereby causing the valve to open. A catching voltage is applied to the lower magnetic coil to ensure the armature is caught. Once the armature has been captured, a holding voltage is applied to hold the valve open. At time t_{ro} the process is reversed in order to close the valve.

The experimental setup consists of the following components; Electromechanical Valve Actuator, Eddy Current Sensor, 2 PWM Drivers, 200 Volt Power Supply, and a Dspace 1103 processing board. The eddy current sensor mounted on the rear of the actuator measures the armature displacement, which is sampled by the Dspace processor at 20 kHz sampling frequency. Based on the displacement and the control algorithm, the Dspace processing

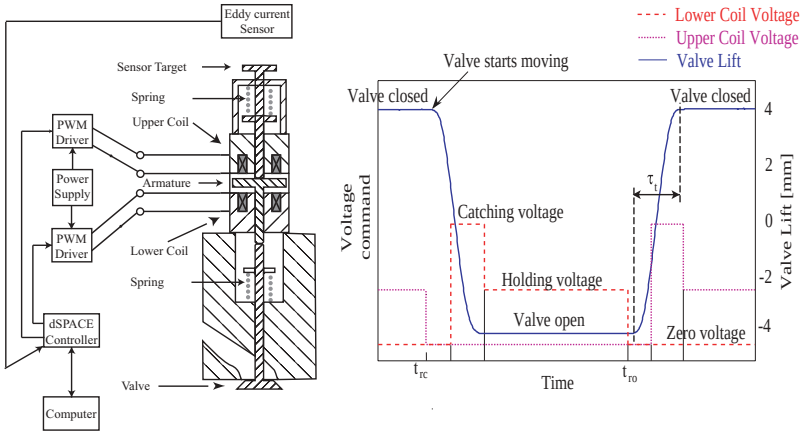

Fig. 1. Electromechanical valve actuator (left) and typical opening/closing cycle (right).

board regulates the PWM frequency to each of the PWM drivers to achieve the desired performance.

While effective in ensuring opening/closing of the valve, the EMV actuator suffers from large impact velocities between the armature, valve, and valve seat leading to excessive noise and wear on the system. The open loop control scheme shown in Fig. 1 results in impact velocities of approximately 1 m/s.

In addition, transition times need to be both quick and consistent to avoid collision with the piston and variability in trapped mass. Before the actuator can be implemented in production vehicles, impact velocities less than 0.1 m/s and transition times of less than 4 ms need to be achieved.

The impact between the armature and catching coil is not a completely elastic collision, and as such the armature will bounce before finally coming to rest against the catching coil. Here, we define the impact velocity to be the largest velocity of the armature when it is in contact with the catching coil. Typically this corresponds to the first collision. The transition time is defined as the time from release to when the armature is 98% closed/open. After it has completed 98% of the travel the additional air let in or out has negligible effects on the engine performance.

3 Soft Landing Methodologies

Various methodologies have been applied in an attempt to achieve soft landing of the EMV actuator. The problem has received considerable attention with the introduction of solenoid-driven actuators [8] and proposed solutions keep on emerging as patents. For example, a search performed in Feb 2002 with keywords *camless*, *engine*, *valve*, *control*, *solenoid* for patents filled in Europe, United States and Japan resulted 303 relevant patents; 37 of which were filled after Sep 2001.

One basic idea is to apply either a pneumatic or hydraulic damper to the system to oppose the motion of the valve. The drawback of such a system is that the extra damping will add to the transition time and power consumption. Another concept is the use of variable rate springs. The spring force would increase as the armature moved near the catching coil, helping to decelerate the armature. A simpler concept would be to use a two-stage spring system, where the second set only effects the last 1-2 mm of travel. Similarly with adding a damper, the modified springs would increase the transition time and power consumption.

Alternatively, feedback could be used to regulate the voltage across the magnetic coils in order to achieve the desired performance. Feedback has the advantage that it would not increase the transition time and the power consumption should be minimized when soft landing is achieved. In [5] the authors use in iterative learning controller (ILC) to modify the feedback from cycle to cycle to decrease the impact velocity. The feedback they start with is not well tuned, resulting in poor performance in the first few cycle before the ILC has had time to adapt. We demonstrate here that it is possible to use a well designed feedback to improve the performance within a single cycle. Using repetitive control, the authors of [13] are able to apply a repetitive learning algorithm to achieve impact velocities with a mean of 0.06 m/s. Unfortunately, due to the use of softer springs, their transition times are quite long (roughly 8 m/s). In [2] the desired impact velocity and transition time are achieved by holding the ratio of the rate of change of current to current at a constant value. Based on the impact velocity of the previous transition the value is modified to improve the response. However, the feedback is based solely on a single point measurement of current and the rate of change of current and as such may not be robust against disturbances.

This paper presents both a linear and nonlinear observer based output feedback controller to achieve the desired performance. In addition, the nonlinear feedback is augmented with a self-tunning algorithm to further improve performance from cycle-to-cycle.

4 Nonlinear Model

The system consists of four states, namely, armature position (z in mm), armature velocity (v in m/s), upper coil current (i_u, in A) and lower coil current (i_l in A). To achieve fast release a reverse polarity voltage technique, described in [15], is used to quickly drive the holding current to zero. Therefore the current in the releasing coil has little influence over the motion of the armature, and as such we can reduce the system from four states to three. Let us define the three state model as: catching coil current (i, in A), distance from the catching coil (z, in mm), and armature velocity (v in m/s). The resulting equations of motion are:

$$\frac{di}{dt} = \frac{V_c - ri + \chi_1(i,z)\,v}{\chi_2(z)} \tag{1}$$

$$\frac{dz}{dt} = 1000v \tag{2}$$

$$\frac{dv}{dt} = \frac{1}{m}\left(-F_{mag}\left(i,z\right) + k_s\left(4-z\right) - bv\right) \tag{3}$$

written compactly as

$$\frac{dx}{dt} = f\left(x, V_c\right), \quad x = \left[\, i \; z \; v \,\right]^T \tag{4}$$

where the catching coil voltage is denoted by V_c in V, the resistance r in Ω, the system mass m in kg, the spring stiffness k_s in N/mm, the damping coefficient b in Ns/m, the magnetic force due to the catching coil F_{mag} in N, the back-emf $\chi_1 v$ in V, and the inductance χ_2 in H.

The magnetic subsystem is characterized by two distinct sets of equations. The boundary between them is defined by the saturation current which is a function of the air-gap distance, $i_x = k_c + k_d z$. When the coil current is less than the saturation current ($i < i_x$) the magnetic force is a quadratic function of the current. The functions χ_1, χ_2, and F_{mag} are given by

$$\chi_1\left(i,z\right) = \frac{2k_a i}{\left(k_b+z\right)^2}, \;\; \chi_2\left(z\right) = \frac{2k_a}{1000\left(k_b+z\right)}, \;\; F_{mag}\left(i,z\right) = \frac{k_a i^2}{\left(k_b+z\right)^2}. \tag{5}$$

If the coil current is greater than the saturation current ($i > i_x$) then the magnetic force no longer increases quadratically with current. Electromagnetic literature refers to this region of operation as the "saturation region". The functions χ_1, χ_2, and F_{mag} are given by

$$\chi_1^{sat}\left(i,z\right) = \chi_1\left(i,z\right)\exp\left(-k_i\left(i-i_x\right)\right) \tag{6}$$

$$\chi_2^{sat}\left(i,z\right) = \chi_2\left(z\right)\exp\left(-i+i_x+i_{min}\right) \tag{7}$$

$$F_{mag}^{sat}\left(i,z\right) = \left(F_{mag}\left(i_x,z\right) - f_{max}\right)\exp\left(-k_i\left(i-i_x\right)\right) + f_{max} \tag{8}$$

where $f_{max} = k_e z + k_f$, $k_i = \frac{\chi_1(i_x,z)}{f_{max} - F_{mag}(i_x,z)}$, and i_{min}, k_a, k_b, k_c, k_d, k_e, and k_f are all constants.

The dynamic behavior due to the impact (bouncing) is included in the model, by extending (3):

$$\frac{dv}{dt} = \frac{1}{m}\left(-F_{mag}\left(i,\, z\right) + k_s\left(4-z\right) - bv + N\right) \tag{9}$$

where N is the normal force acting between the armature and catching coil. The force N is given by

$$N = \begin{cases} \text{if } z \neq 0, & 0 \\ \text{if } z = 0, & \begin{cases} \text{if } v = 0, & F_{mag}\left(i,\, 0\right) - 4k_s \\ \text{if } v \neq 0, & \begin{cases} \text{if } v < 0, & \delta \\ \text{if } v > 0 & 0 \end{cases} \end{cases} \end{cases} \tag{10}$$

where δ is an impulse function calibrated to give $v^+ = ev^-$, where v^+ is the velocity just after impact and v^- is the velocity just before impact. The parameter $e < 1$ is chosen based on experimental data and represents the loss of kinetic energy due to the plastic collision.

Comparison of the model response and experimental data is shown in Fig. 2. The data is generated by using a 120 V catching voltage applied to the lower coil 1 ms after the armature is released from the upper coil.

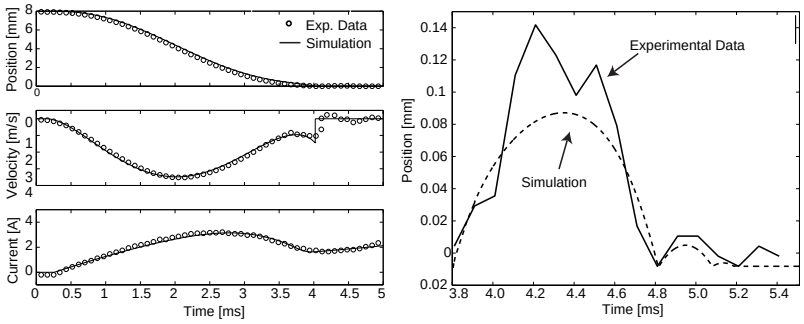

Fig. 2. Comparison of the model to experimental data (left) and the impact detail (right).

5 Control Analysis

In this section a detailed dynamical analysis of the system is presented using nonlinear and linear (small signal) analysis around equilibria. The results presented here will serve as the basis for the various controller designs presented in Section 7.

5.1 Stability

An equilibrium position is defined by the voltage that results in a constant current with magnetic force equal to the spring force. Fig. 3 shows the magnetic force for four different values of current and the spring force as a function of position. Their intersection defines four equilibrium points. Analysis of the system demonstrates that all the equilibria near $z = 0$ are unstable. A perturbation from equilibrium which decreases z will accelerate the armature toward the coil seat as the spring force increases linearly while the magnetic force increases quadratically with the decreasing position. This acceleration can result in high impact velocities if the current is not rapidly adjusted to a lower value. On the other hand, a perturbation which increases z will reduce the magnetic force and the spring will therefore push the armature toward the middle position where the equilibria are stable.

The addition of the normal force to (9) not only adds impact dynamics, but also explicitly shows the multiple equilibria of the system at the contact point. The system is at equilibrium for the set of states and inputs

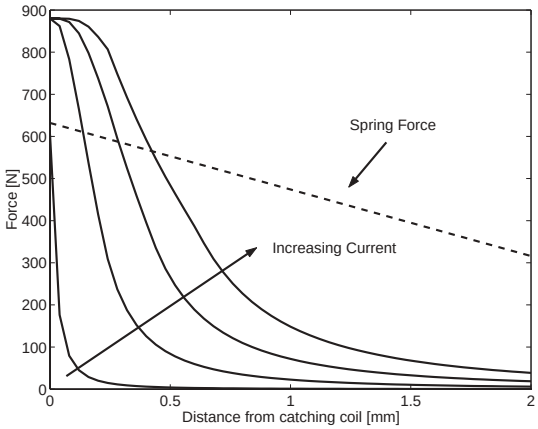

Fig. 3. Magnetic force for several values of current.

$$x_e = \{[i,\, z,\, v] \mid i \geq i_e,\, z = 0,\, v = 0\} \tag{11}$$

$$i_e = \{i \mid F_{mag}\,(i, 0) = 4k_s\}\,,\; V_c = \frac{i}{r}. \tag{12}$$

This is a very important result for controller design considerations. Specifically:

- If there exists an infinite set of equilibrium points, all of which result in the armature being held against the magnetic coil, which one should the controller drive the system to?
- If linear control theory is to be used, which equilibria should be selected to linearize the system about?

The answer to the first question should be based on a trade-off between robustness against bouncing and power consumption. An equilibrium point, defined by (11), that uses a small holding current runs the risk of losing the armature due to bouncing and/or disturbances acting on the valve. The smallest of the four magnetic force curves in Fig. 3just barely exceeds the spring force when the armature is in contact with the catching coil. Therefore the current corresponding to this curve should be sufficient to hold the armature against the magnetic coil. However, a small deviation in position reduces the magnetic force more than the spring force. If the armature were to bounce due to impact the magnetic force would no longer be great enough to hold the armature in place.

On the other hand, a large holding current will increase the power consumption of the actuator and can potentially eliminate the projected fuel economy benefits of an engine equipped with a VVT system. Three times the minimum holding current is selected and used in the sequel. A combined

design-optimization study needs to be performed to rigorously address this question in the future.

5.2 Control Difficulties

The system suffers from low control authority in controlling the armature position from the voltage input throughout the executed motion. The underlying reasons are dynamic during small gaps and static during large gaps. Specifically, during small gaps the low control authority arises from the decreased inductance combined with the increased back-emf that drives the current to zero exceedingly fast. During large gaps the magnetic force is not strong enough to balance the spring force. These phenomena need to be understood in order to design a successful controller.

Let us first consider the small gaps where the current is less than the saturation current, and then substitute (5) into (1). The resulting equation is a first order approximation of the current dynamics.

$$\frac{di}{dt} = 1000\left(\frac{(V_c - ri)\,(k_b + z)}{2k_a} + \frac{iv}{(k_b + z)}\right) \tag{13}$$

Note that $k_b \ll 1$ and z is approaching zero. Let us replace the term $k_b + z$ with the small parameter $\varepsilon = k_b + z$, resulting in

$$\frac{di}{dt} = 1000\left(\frac{(V_c - ri)\,\varepsilon}{2k_a} + \frac{iv}{\varepsilon}\right) \quad \text{or} \quad \varepsilon\frac{di}{dt} = 1000\left(\frac{(V_c - ri)\,\varepsilon^2}{2k_a} + iv\right) \tag{14}$$

Two observations should be made from (14). First, the input voltage is being multiplied by ε, therefore very near the catching coil, the voltage cannot easily affect the current dynamics. Second if we multiply through by ε we see that the current dynamics become singularly perturbed near the catching coil. For $z > 1$ mm these affects aren't present as ε is greater than 1.

When the gap is greater than approximately 1 mm the catching coil lacks control authority over the motion of the armature because the magnetic force is much less the spring force as shown in Fig. 3. Therefore the system response is dominated by the springs. Despite this, it is necessary to apply voltage to the catching coil while the armature is not near it. If voltage is not applied to the system until the armature is close to the catching coil, it will be extremely difficult to raise the current because of the back-emf. It is much easier to raise the current before the system becomes singularly perturbed, and then apply large inputs near the end of the transition to overcome the current decaying effects from the back-emf seen in equation (14).

5.3 Small Signal Analysis

To capture the system dynamics throughout a complete transition, we linearize the system about two different equilibria to obtain two linear models, which will henceforth be refer to as

- **near model**, which is valid for $z \in (0, 1)$ mm.
- **far model**, which is valid elsewhere.

The far model is derived by linearizing the system at an equilibrium point slightly away from the mid-position. For the first 7 mm of the transition the mechanical and electrical subsystems of the EMV actuator are essentially a decoupled mass-spring-damper and RL circuit respectively. The far model is used to capture this behavior.

Near the catching coil, the mechanical and electrical subsystems are no longer decoupled as the magnetic force has influence over the armature motion and the back-emf and changing inductance become significant. From Fig. 3 we see that linearizing the system at i_e will cause the near model to be highly unstable as the magnetic force drops off to a much smaller value than the spring force due to a small deviation in position. A higher value of equilibrium current will result in a near model that is (i) a better approximation of the nonlinear system behavior, and (ii) a safer equilibrium point since it can account for small normal forces during bouncing.

Both the near and far model have the structure

$$\frac{d}{dt}\begin{bmatrix} \Delta i \\ \Delta z \\ \Delta v \end{bmatrix} = \begin{bmatrix} a_{11} & 0 & a_{13} \\ 0 & 0 & a_{23} \\ a_{31} & a_{32} & a_{33} \end{bmatrix} \begin{bmatrix} \Delta i \\ \Delta z \\ \Delta v \end{bmatrix} + \begin{bmatrix} b_1 \\ 0 \\ 0 \end{bmatrix} \Delta V_c \tag{15}$$

written compactly as $\frac{d}{dt}\Delta x = A\Delta x + B\Delta V_c$, where A and B have different values for the near and far region. Note that the term a_{12} is zero indicating that the rate of change of current, $\frac{d\Delta i}{dt}$ does not depend on position, although (13) clearly shows strong dependency in position in non-equilibrium conditions. Indeed, linearization around any equilibrium point will result in $\frac{d\Delta i}{dt}$ not being a function of position as shown below.

Taking the partial derivative of (1) with respect to position yields

$$\frac{\partial}{\partial z}\frac{di}{dt} = \frac{\left(v\frac{d}{dz}\chi_1\right)\chi_2 - \left(V_c - ri + \chi_1 v\right)\frac{\partial}{\partial z}\chi_2}{\left(\chi_2\right)^2}. \tag{16}$$

To satisfy equilibrium conditions the velocity must be zero, $v = 0$ and the applied voltage must equal to the voltage drop in the resistance, $V_c = ri$. Thus, the terms in both parentheses in the numerator of (16) will be zero, and consequently, $\frac{\partial}{\partial z}\frac{di}{dt} = 0$ when evaluated at any equilibrium point.

From (14) we know that this only presents a problem for the near model where the current becomes singular perturbed. For large values of z, the changing inductance and back-emf are negligible and are of no consequence. As z approaches zero, the changing inductance and back-emf are no longer negligible and must be taken into account.

To account for the singularly perturbed current dynamics present in the non-equilibrium full nonlinear equations during small gaps, we assume cur-

rent reaches its steady state solution $\Delta i^* = -\frac{a_{13}\Delta v + b_1 \Delta V_c}{a_{11}}$ governed by the fast stable dynamics of the near model:

$$\frac{d\Delta i}{dt} = 0 = a_{11}\Delta i + a_{13}\Delta v + b_1 \Delta V_c, \tag{17}$$

resulting in the reduced state space representation

$$\frac{d}{dt}\begin{bmatrix}\Delta z \\ \Delta v\end{bmatrix} = \begin{bmatrix}0 & a_{12}^* \\ a_{21}^* & a_{22}^*\end{bmatrix}\begin{bmatrix}\Delta z \\ \Delta v\end{bmatrix} + \begin{bmatrix}0 \\ b_2^*\end{bmatrix}\Delta V_c. \tag{18}$$

Recall that the rate of change of current is approaching large negatives values and thus can be neglected from the control design for the linear near model. This is also verified by the fact that the original a_{11} term in (15) is Hurwitz.

6 Observer Design

High cost and implementation issues preclude the use of sensors to measure all three states. For each of the controllers presented later in Sect. 7 only a position sensor is used, and an observer is implemented to estimate velocity and current. Unfortunately, the observability matrix $\begin{bmatrix} C^T & (CA)^T & (CA^2)^T \end{bmatrix}^T$ where A is from the far model and $C = \begin{bmatrix} 0 & 1 & 0 \end{bmatrix}$, is ill-conditioned. Therefore one or more states are weakly observable from the position measurement.

From the physics of the system it is obvious that current is the weakly observable state. For the majority of the armature travel the magnetic force, and thus current, has little influence over the armature motion (i.e. the system output). Although this is to be expected for the far model, it is important to note that using the near model will also result in an ill-conditioned observability matrix. At small distances the magnetic force is influenced by changes in position more than changes in current. Thus the affect of current on the output is still weakly observable.

Only the far model is used to design the observer. Of the two linear models, the far model is valid for almost the entire range of motion. Rather than deal with the difficulties of switching between two dynamical observers, the output injection term is used to ensure accuracy of the state estimates.

Setting $a_{31} = 0$, which is small in comparison to a_{32} and a_{33}, removes $\frac{d\Delta v}{dt}$ dependence on current. The new state space matrix, $\widetilde{A}$, is given by

$$\widetilde{A} = \begin{bmatrix}a_{11} & 0 & a_{13} \\ 0 & 0 & a_{23} \\ 0 & a_{32} & a_{33}\end{bmatrix} = \begin{bmatrix}A_{\overline{o}} & A_{12} \\ 0 & A_o\end{bmatrix}. \tag{19}$$

The system can now be decomposed into observable and unobservable parts, A_o and $A_{\overline{o}}$ respectively.

Using the nonlinear model presented in [15] a nonlinear exponential detector is implemented as

$$\frac{d\widehat{x}}{dt} = f\left(\widehat{x}, V_c\right) + L\left(y - \widehat{y}\right), \tag{20}$$

where, the function $f(\widehat{x}, V_c)$ is the same as (4) except that it does not includ the saturation dynamics in (6)-(8). The matrix L is given by $L = \begin{bmatrix} 0 \, l_1 \, l_2 \end{bmatrix}^T$, where l_1 and l_2 are tuned based on linear quadratic estimation methods on A_o and $C_o = \begin{bmatrix} 1 \, 0 \end{bmatrix}$.

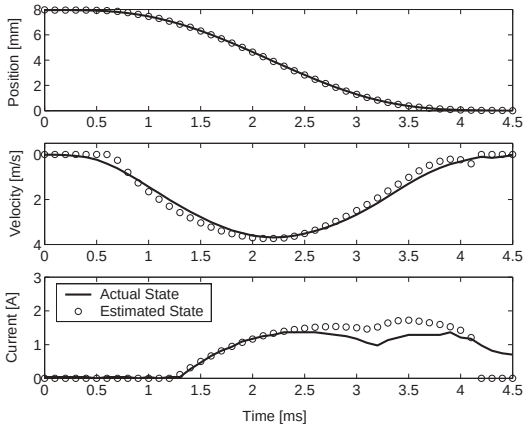

Fig. 4. Comparison of the estimated vs. actual states.

A comparison of the actual and estimated states is presented in Fig. 4. The observer is able to estimate position and velocity with very little error. The current estimate matches the actual state closely for the initial part of the transition, with the estimation error increasing toward the end. Recall that (20) does not include the saturation region in (6)-(8), thus at the end of the transition when saturation occurs the nonlinear model is not accurate. Additionally the current estimate is running open loop therefore output injection can not be used to drive the estimation error to zero.

7 Controller Design

This section presents various controllers implemented to achieve soft landing of an EMV actuator. The control difficulties outlined in Sec. 5.2 imply that for a controller to be successful it must:

1. Apply voltage during the initial motion of the armature to raise the coil current and establish a magnetic field as the armature approaches the catching coil. The strong magnetic field helps to compensate for the inevitable current drop caused by the back-emf and changing inductance near the catching coil.
2. Apply large voltage near the catching coil to avoiding bouncing and to compensate for the decreasing current and reduced influence of the voltage on the current dynamics.

7.1 Linear Controller

The linear controller uses the feedback, $u = u_{eq} - K\Delta\widehat{x}$. Where $u_{eq} = \frac{i_{des}}{r}$, i_{des} is the desired current value, typically 0.5-1.5 A, that the controller drives the current to, $\Delta\widehat{x} = \widehat{x} - x_e$, $\widehat{x}$ is the estimate of the actual state, and x_e is the equilibrium point. The gain matrix, K, is determined by using the Linear Quadratic Regulator (LQR) methodology with diagonal weighting matrices Q and R.

Just as two linear models are used to capture the system dynamics, the linear controller is split to compensate for the changing system dynamics. The two controller stages are named: "Flux Initialization" and "Landing".

Stage 1 Controller, Flux Initialization: To overcome the problems inherent to the current dynamics it is desirable to bring the current near a nominal catching value before the armature approaches the catching coil. On one hand, if the current is not brought up before the armature approaches the catching coil, it will be difficult to do so later due to the reasons explained in Sect. 5.2. On the other hand, closed loop control during this time may result in actuator saturation as the magnetic force has low authority over the armature motion for $z > 1$ mm.

To improve robustness within a cycle, our controller uses the flux initialization stage to apply closed loop control throughout the travel $z \in (1, 8)$ mm. Using the far model, the weighting matrices in the LQR method are chosen to penalize deviations from the nominal catching current much more than deviations in position or velocity. Since the actuator has control authority over current, actuator saturation is avoided. Additionally, robustness is improved as the controller can compensate for variations in both position and velocity.

Stage 2 Controller, Landing: As the armature approaches the catching coil, the controller switches to the second stage at $z = 1$ mm. The landing controller catches the armature and brings it into contact with the coil while attempting to minimize the impact velocity.

The reduced order near model, given in (18), is used in the LQR method to design the landing controller. In (15), a_{11} is Hurwitz, and consequently the current dynamics are stable. Therefore we need only design a stabilizing feedback for the reduced order model.

A typical soft landing is presented in Fig. 5. The impact velocity represents a factor of six reduction over the open loop control. Statistical data for the impact velocity is listed in Table 1. The controller achieves a transitions time with a mean of 3.42 ms. The standard deviation, σ, is 0.2 ms, and the maximum and minimum transition times are 4.3 ms and 3.3 ms respectively.

7.2 Nonlinear Controller

Equation (14) shows the sever limitations of linear control methodologies for the EMV actuator. In a linear controller the input voltage is proportional to the error (i.e. $V_c = Kz$) exacerbating the decrease of the influence of the

input voltage as z approaches zero. Thus large values of the gain, K, will be required to overcome the changing current dynamics. This can, and does lead to actuator saturation as shown in Fig. 5. Moreover, it leads to small voltage inputs near the catching coil, potentially creating problems with bouncing.

To overcome the changing current dynamics and reduced control authority we propose the use of a nonlinear controller of the form

$$V_c = \frac{K_1}{\gamma + z} v + \frac{K_2}{\beta + z}. \tag{21}$$

The control input is inversely proportional to the distance from the catching coil, thereby alleviating the affect of the decreasing influence of the voltage on the current dynamics. The parameters K_1, K_2, γ, and β are used to tune the controller to achieve the desired performance.

Since the current is not driven near the minimum equilibrium value, the magnetic force will remain larger than the spring force for small bounces. Thereby eliminating the potential loss of the armature due to bouncing.

Even thought the nonlinear controller does experience actuator saturation, the affect is much smaller than that caused by the linear controller. Whereas the linear controller causes voltage saturation before the valve is fully open/closed, the nonlinear controller does so only at the very end of the transition.

Experimental results in Fig. 5 and Table 1 show that the controller achieves a mean impact velocity of 0.16 m/s. Similar to the linear controller, the nonlinear controller represents a factor of six reduction over the open loop control. The nonlinear controller achieves a mean transition time of 3.23 ms. Although the mean values achieved with the nonlinear controller are similar to the ones achieved with the linear controller, the results are more consistent as indicated by the standard deviation, $\sigma = 0.04$ ms, and the maximum and minimum transition times which are 3.3 ms and 3.2 ms respectively.

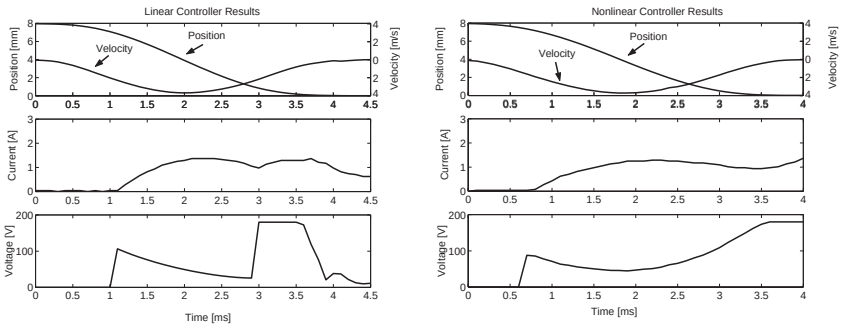

Fig. 5. Experimental results achieved by using the linear (left) and nonlinear controller (right).

8 Extremum Seeking Control

So far the controller design has only considered closed loop compensation during a single transition. By applying a tunning algorithm from cycle to cycle it is possible to improve the performance of the actuator and adjust the controller parameters to account for changes in the system due to environmental variations. Here, an extremum seeking controller [7] is used to tune the feedback between each transition to minimize the impact velocity.

Applying extremum seeking control to a static nonlinearity minimizes or maximizes the system output, J. While the EMV actuator with nonlinear feedback is not a static nonlinearity, it can be treated as such. If one of the four parameters K_1, K_2, γ, or β of the nonlinear feedback is taken to be the input and the impact velocity or another relevant function is used as the output, J. To account for the delay between the start of the valve transition and the armature impacting against the catching coil, the extremum seeking control is discretized with a sampling rate equal to the rate of the valve transitions.

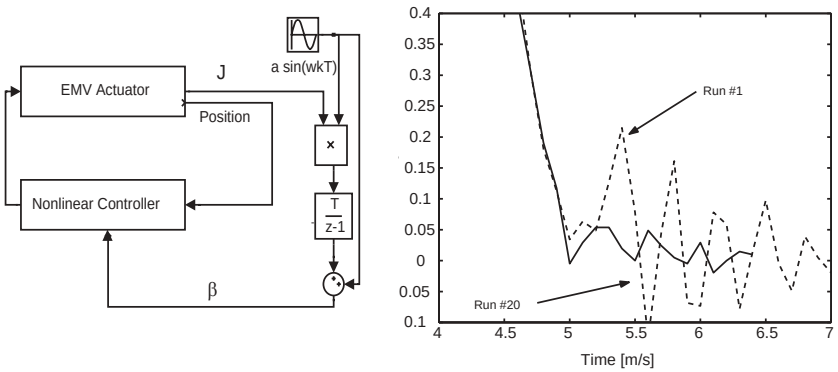

Fig. 6. Extremum seeking feedback as applied to the EMV actuator (left), and extremum seeking feedback results (right).

The parameter β, has a very strong influence on the impact velocity, v_I, and is therefore selected as the input. This method does not depend on measuring the impact velocity, which could be impractical and expensive. All that is required is an output that is proportional to the impact velocity in order to determine whether or not the previous impact velocity was larger or smaller. Here a small microphone is used to pick off the sound caused by the impact and the extremum seeking control is set to maximize the function $J = -(S_{min} - S_{meas})^2$. Where S_{min} is the desired sound level, and S_{meas} is the measured sound level. Note that S_{min} needs to be carefully set to a non-zero value otherwise the extremum seeking control will minimize the sound intensity by avoiding any contact which is obviously not desired. The output

function can be generated by a variety of other sensors that relate to the impact velocity such as accelerometers, load washers, and knock sensors.

To test the extremum seeking control the feedback is initialized at a non-optimal value of β and allowed to run, the results are shown in Table 1 and Fig. 6. By compensating for the day to day variations in the system the extremum seeking control has improved the system performance by a factor of 2. More details on this algorithm can be found in [11].

Table 1. Impact velocities achieved by the different controllers.

	Linear Controller	Nonlinear Controller	Extremum Seeking
Mean	0.16 m/s	0.16 m/s	0.08 m/s
σ	0.09 m/s	0.08 m/s	0.05 m/s
Max	0.35 m/s	0.32 m/s	0.20 m/s
Min	0.06 m/s	0.05 m/s	0.05 m/s

9 Conclusion

The EMV actuator presents an interesting and challenging control design problem. The controller must achieve stringent performance requirements for soft and fast landing (impact velocities below 0.1 m/s and transition time smaller than 4.0 ms). The input-to-output behavior is nonlinear with low control authority for a combination of reasons that once understood a practical control solution arises.

Despite the improvement in impact velocity presented here, much work remains to be done. Before the EMV actuator can be used on a firing engine, the controller must be able to compensate for gas forces acting on the valve due to the combustion in the cylinder and any valve lash that may be present to compensate for the thermal expansion between the valve stem and the armature.

References

1. Ahmad T and Theobald MA. A Survey of Variable Valve Actuation Technology. *SAE* 891674.
2. Butzmann S., Melbert J., and Koch A., "Sensorless Control of Electromagnetic Actuators for Variable Valve Train," SAE Paper No. 2000-01-1225.
3. Hatano K., Iida K., Higashi H., and Murata S., "Development of a New Multi-Mode Variable Valve Timing Engine", SAE Paper No. 930878, 1993.
4. Hrovat D. and Powers W. F., "Modeling and Control of Automotive Powertrains", Control and Dynamic Systems, Vol. 37, pp. 33-64, 1990.
5. Hoffmann W., Stefanopoulou A., "Iterative Learning Control of Electromechanical Camless Valve Actuator," Proceedings American Control Conference, pp.2860-2866, June 2001.

6. Kreuter P., Heuser P., and Schebitz M., "Strategies to Improve SI-Engine Performance by Means of Variable Intake Lift, Timing and Duration", SAE Paper No. 920449 , 1992.
7. Krstic M., Wang H.H., "Stability of extremum seeking feedback for general nonlinear dynamic systems," Automatica, vol. 36, pp595-601, 2000.
8. R. B. Mathews, "Electromagnetic Control Device," United States Patent 2,769,943, August 22, 1949.
9. Moriya Y., Watanabe A., Uda H., Kawamura, H., and Yoshioka M., "A Newly Developed Intelligent Variable Valve Timing System- Continuously Controlled Cam Phasing as Applied to a New 3 Liter Inline 6 Engines", SAE Paper No. 960579, 1996.
10. Peterson, K., Stefanopoulou A., Haghgooie M., Megli, T. "Output Observer Based Feedback for Soft Landing of Electromechanical Camless Valvetrain Actuator", Proceedings of American Control Conference, pp. 1413-1418, May 2002.
11. Peterson K., Stefanopoulou A., Wang Y., Megli T., Haghgooie M., "Nonlinear Self-Tuning Control for Soft Landing of an Electromechanical Valve Actuator," to be presented at the 2002 IFAC on Mechatronics.
12. Schechter M. M. and Levin M. B., "Camless Engine", SAE Paper No. 960581, 1996.
13. Tai C., Stubbs A., Tsao T.C., "Modeling and Controller Design of an Electromagnetic Engine Valve," Proceedings of American Control Conference, pp. 2890-2895, June 2001.
14. Titolo A., "The Variable Valve Timing System - Application on a V8 Engine", SAE Paper No. 910009, 1991.
15. Wang Y., Stefanopoulou A., Peterson K., Megli T., Haghgooie M., "Modeling and Control of Electromechanical Valve Actuator," SAE 2002-01-1106